fire

MDPI

Article

Simplified Post-Fire Structural Performance of Biaxial Voided Reinforced Concrete Slabs: Influence of Void Geometry

Nursel Kütük * and Mustafa Özakça *

Department of Civil Engineering, Gaziantep University, Gaziantep 27310, Turkey
* Correspondence: kutuknursel@gmail.com (N.K.); ozakca@gantep.edu.tr (M.Ö.)

Abstract

Reinforced concrete (RC) slabs with internal voids are increasingly used to improve material efficiency; however, their residual structural performance after fire exposure remains insufficiently understood. This study presents a numerical investigation of RC slabs with different void geometries using a three-dimensional nonlinear Finite Element (FE) model. A sequential thermal–structural approach was adopted, in which fire exposure was simulated through transient thermal analysis, and the resulting spatial distribution of maximum temperatures was used to assign residual material properties to each FE based on its local peak temperature, followed by structural analysis under ambient conditions. A parametric study was conducted on seven slab configurations, including two solid slabs and five voided slabs with spherical, elliptical, ellipsoidal, capsule, and biaxial capsule geometries. To ensure a consistent evaluation, two reference solid slabs were considered: a 230 mm thick slab to enable comparison under identical geometric conditions, and a 160 mm thick slab representing equivalent concrete volume to assess material efficiency. Fire exposure was applied according to the ISO 834 standard fire curve for durations of 30, 60, and 90 min. The results indicate that voided slabs exhibit higher deflections than the solid slab of identical thickness due to reduced stiffness, while achieving comparable performance relative to the solid slab with equivalent concrete volume. These findings highlight the trade-off between structural stiffness and material efficiency under increasing fire exposure time.

Keywords: fire exposure; voided slab systems; reinforced concrete slabs; post-fire behavior; thermo-structural analysis; finite element analysis

1. Introduction

Biaxial voided slabs are increasingly adopted as an efficient structural solution that reduces self-weight and material consumption while maintaining adequate stiffness and load-carrying capacity [1–6]. By replacing structurally inefficient concrete in the core region with lightweight void formers, these systems can reduce concrete volume by up to 30–40%, providing both structural efficiency and environmental benefits [7,8]. However, despite their growing application in modern construction, their behavior under fire exposure remains insufficiently investigated.

Previous research has primarily focused on the structural performance of voided slabs under ambient conditions, particularly in terms of flexural behavior, punching shear capacity, and serviceability performance [9–15]. These studies generally demonstrate that voided slabs can achieve structural performance comparable to conventional solid slabs despite reduced material usage. Nevertheless, most existing investigations are limited to

Check for updates

Academic Editor: Ali Cemal Benim

Received: 6 April 2026
Revised: 7 May 2026
Accepted: 8 May 2026
Published: 15 May 2026

Copyright: © 2026 by the authors. Licensee MDPI, Basel, Switzerland. This article is an open access article distributed under the terms and conditions of the Creative Commons Attribution (CC BY) license.

ambient temperature conditions (i.e., without thermal loading or fire exposure) and do not account for the effects of elevated temperatures.

RC structures are generally considered to exhibit good fire resistance due to their ability to retain structural integrity under high temperatures [16]. At the material level, exposure to elevated temperatures leads to significant microstructural changes in concrete, resulting in reductions in strength and stiffness [17–19]. Notably, the residual strength after cooling may be lower than the strength during heating due to irreversible damage mechanisms such as dehydration and micro-cracking [17]. In addition, the thermo-mechanical response of concrete exhibits considerable variability depending on material composition and testing conditions [19]. Consequently, both concrete and reinforcing steel experience degradation in mechanical properties under fire exposure, leading to reductions in stiffness and load-carrying capacity of RC members.

The presence of internal voids may further influence heat transfer mechanisms and temperature distribution within the slab, thereby affecting the extent and distribution of thermal damage and the resulting structural response. Several experimental studies have investigated the behavior of voided slabs after exposure to high temperatures, reporting significant reductions in residual strength, stiffness, and ductility with increasing temperature levels [20,21]. Experimental investigations on bubble deck slabs subjected to different fire temperatures and durations have also demonstrated considerable degradation in load-carrying capacity, accompanied by changes in failure modes [22]. In addition, numerical studies have been conducted to simulate the thermo-mechanical response of voided slab systems under fire conditions using FE methods [23]. However, existing studies remain limited and do not provide a comprehensive understanding of the residual structural behavior of biaxial voided slabs, particularly with respect to the influence of void geometry.

In this context, the present study develops a three-dimensional nonlinear FE model to investigate the residual structural response of RC slabs with different void geometries following fire exposure. A systematic comparison was carried out on seven full-scale slab configurations, including two solid slabs (160 mm and 230 mm thick) and five voided slabs with spherical, elliptical, ellipsoidal, capsule, and biaxial capsule geometries. To ensure a consistent and meaningful evaluation, two comparison approaches were adopted:

(i) slabs with identical thickness (230 mm) to isolate the influence of void geometry on structural behavior, and
(ii) slabs with equivalent concrete volume, in which the 160 mm thick solid slab represents the same concrete volume as the 230 mm voided slabs, allowing assessment of material efficiency independent of geometric stiffness.

Fire exposure was applied in accordance with the ISO 834 standard fire curve [24] for durations of 30, 60, and 90 min, representing increasing levels of thermal damage. The structural response was subsequently evaluated under uniformly distributed loading conditions to assess residual deformation behavior. It should be noted that the analysis focuses on deformation-based performance under service-level loading. Residual stresses induced during the heating and cooling phases were not explicitly modeled; instead, temperature-dependent material degradation was incorporated into the structural analysis to represent the effects of fire exposure. The developed model was validated against available experimental data and subsequently employed to evaluate the role of void geometry in governing both structural behavior and material efficiency after fire exposure.

2. FE Model Development and Validation Using Experimental Data

The FE method can effectively simulate structural performance, provided that geometry, material properties, boundary conditions, and loading configurations are accurately defined. This is particularly important for RC members, whose response is governed

by highly nonlinear material behavior, especially under elevated temperature conditions. Therefore, prior to conducting the parametric study, the FE model was systematically validated against available experimental data to ensure its predictive reliability.

In the present study, a three-dimensional nonlinear FE model was developed in ANSYS Workbench 2022 R1 [25] to simulate the structural behavior of biaxial voided RC slabs subjected to fire exposure. The numerical model was validated against the experimental results reported by Al-Gasham et al. [20], specifically the BS-500 and BS-800 specimens exposed to fire for 60 min. To the best of the authors' knowledge, experimental or numerical datasets for fire-exposed voided slabs remain very limited, and many existing studies do not provide sufficient detail for reliable reproduction. In addition, the thermal response was further assessed by comparing the through-thickness temperature distribution of solid slabs with the provisions of EN 1992-1-2 [26], as presented in Section 4.

The validation process involved replicating the experimental conditions, including geometry, reinforcement detailing, boundary conditions, and loading configuration. Temperature-dependent material properties were defined in accordance with EN 1992-1-2 [26], particularly Sections 3.2 and 3.3 for concrete, and EN 1993-1-2 [27], particularly Sections 3.2 and 3.4 for reinforcing steel. The load–deflection responses obtained from the FE analysis were then compared with the corresponding experimental results to evaluate the predictive capability of the model.

The FE analyses were performed in ANSYS Workbench [25] using a sequential thermal–structural framework. The thermal response was simulated using SOLID278 elements, while the structural response was modeled using SOLID185 elements for concrete and REINF264 elements for reinforcement. The analysis was conducted using the standard element formulations available in the software, without employing APDL-based user-defined material models or advanced constitutive formulations specifically developed for RC.

This modeling approach provides a robust and computationally efficient framework for thermo-structural analysis and is well suited for capturing global structural behavior and temperature-dependent material degradation. However, it should be noted that the default material formulations do not explicitly represent certain aspects of RC behavior at service load levels, particularly tension softening and distributed cracking mechanisms. As a result, cracking-induced stiffness degradation may not be fully captured in the pre-peak response.

Nevertheless, since the same modeling framework is consistently applied across all slab configurations, the numerical results provide a reliable basis for the comparative evaluation of structural performance, which constitutes the primary objective of the present study.

It should also be noted that residual stresses generated during the heating and cooling phases were not explicitly considered. A sequential thermal–structural approach was adopted, in which a transient thermal analysis was first performed to determine the temperature field within the slab. The resulting spatial distribution of maximum temperatures was then used to assign residual material degradation to each FE based on its local peak temperature. The subsequent structural analysis was conducted under ambient conditions, assuming that the slab had fully cooled to room temperature. Accordingly, thermal strains were not included in the mechanical analysis, and the computed response represents the residual structural behavior governed by stiffness reduction and irreversible material degradation following fire exposure.

2.1. Geometry and FE Mesh

The numerical models were constructed based on the exact geometric dimensions of the tested slabs, namely 500 mm length, 270 mm width, and 90 mm thickness. Fifteen spherical voids with a diameter of 70 mm were modeled and arranged between the top and bottom reinforcement meshes, each consisting of 6-Ø4 mm bars in short direction and 10-Ø4 mm bars in the long direction, maintaining the same spacing and configuration described in the experimental program as shown in Figure 1.

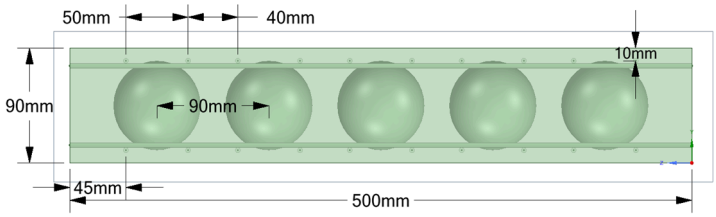

Figure 1. Geometry of the biaxial voided slab specimens FE model developed in ANSYS Workbench.

The concrete domain, including the spherical voids, was modeled using three-dimensional solid elements (SOLID185 in the structural analysis and SOLID278 in the thermal analysis), while the reinforcement was represented using embedded line elements (REINF264), using the standard element formulations available in ANSYS Workbench.

The internal voids were modeled as empty cavities without assigned mechanical stiffness or load-carrying capacity. In the thermal analysis, these regions were treated as air-filled spaces. The material properties of the void formers were not explicitly modeled, as their mechanical contribution is negligible compared to the surrounding concrete. Accordingly, the voids were idealized as non-structural regions to enable a direct evaluation of material efficiency.

A structured meshing strategy with predominantly hexahedral elements was adopted to ensure numerical stability and stress distribution. The meshing approach followed the methodology reported by Miller et al. [23], where a uniform hex mesh configuration was successfully applied for fire-exposed spherical void slabs. As illustrated in Figure 2, the maximum element size (edge length) was limited to 15 mm in the concrete domain to enhance accuracy in regions with geometric discontinuities. The reinforcement was discretized using embedded line elements with a compatible element size. The same meshing strategy and element size control were consistently adopted for BS-800 models to provide direct comparability during the validation process.

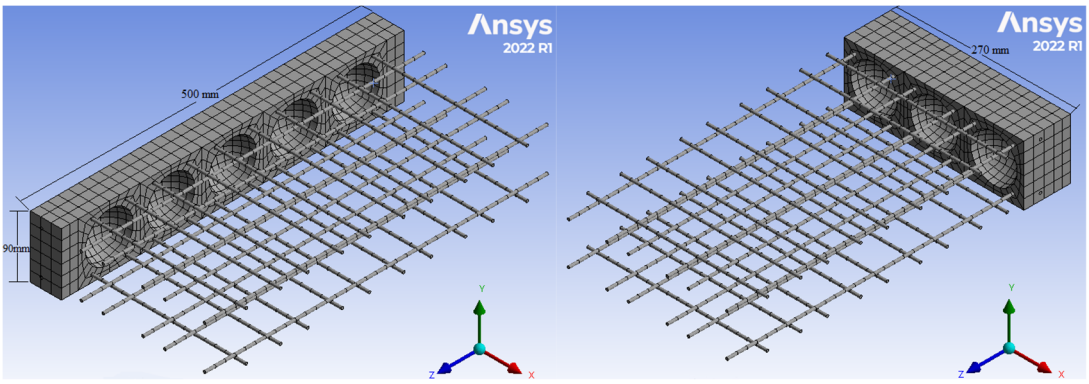

(**a**) (**b**)

Figure 2. FE mesh of the biaxial voided slab model showing internal voids and reinforcement details: (**a**) longitudinal view (500 mm direction); (**b**) transverse view (270 mm direction).

2.2. Material Modeling

The thermo-mechanical response of RC was simulated using a sequentially coupled FE framework, in which the transient thermal field was first obtained and subsequently used to define temperature-induced material degradation for the structural analysis. Temperature-dependent material properties for both concrete and reinforcing steel were defined in accordance with Eurocode provisions.

Concrete: The constitutive behavior of concrete under compression was described using a temperature-dependent elastoplastic model formulated in terms of effective stress. The uniaxial compressive response was defined by a nonlinear stress–strain relationship, while the tensile strength was estimated from the measured compressive strength. The stress–strain relationship in compression is expressed as:

$$\sigma_c = f_c(T).\phi(\varepsilon_c,\ T) \tag{1}$$

where $f_c(T)$ is the temperature-dependent compressive strength and $\phi(\varepsilon_c,\ T)$ represents the nonlinear strain function. The ambient temperature compressive strength of concrete was taken as 24.8 MPa, directly adopted from the experimental program reported by Al-Gasham et al. [20]. The elastic modulus $E_c(T)$, compressive strength $f_c(T)$, and tensile strength $f_t(T)$ were reduced as functions of temperature in accordance with EN 1992-1-2 [26].

The transient heat transfer within concrete was governed by the heat conduction equation:

$$\rho_c(T)c_c(T)\frac{dT}{dt} = \nabla.(k_c(T)\nabla T) \tag{2}$$

where $\rho_c(T)$, $c_c(T)$, and $k_c(T)$ denote density, specific heat capacity, and thermal conductivity, respectively.

Combined convective and radiation heat transfer at the exposed boundary was modeled such that:

$$-k_c(T)\nabla T * n = h(T_s - T_g) + \varepsilon\sigma\left(T_s^4 - T_g^4\right) \tag{3}$$

where $k_c(T)$ is the temperature-dependent thermal conductivity of concrete, n is the outward normal vector, h is the convective heat transfer coefficient, T_s is the slab surface temperature, T_g is the surrounding gas temperature, ε is the surface emissivity, and σ is the Stefan–Boltzmann constant. Thus, radiation was not neglected in the thermal analysis; it was included together with convection in the boundary heat transfer model. However, radiative heat exchange between the internal surfaces of the void cavities was not explicitly considered. The adopted temperature-dependent thermal property functions are shown in Figure 3.

Reinforcing Steel: The reinforcing steel was modeled using a temperature-dependent bilinear elastoplastic constitutive law with perfectly plastic post-yield behavior. The uniaxial stress–strain relationship is given by:

$$\sigma_s = \begin{cases} E_s(T)\varepsilon_s & for\ \varepsilon_s \le \varepsilon_y(T) \\ f_y(T) & for\ \varepsilon_s > \varepsilon_y(T) \end{cases} \tag{4}$$

where $E_s(T)$ is the temperature-dependent elastic modulus and $f_y(T)$ is the temperature-dependent yield strength. The ambient temperature yield strength of reinforcing steel was taken as 508 MPa, consistent with the material properties reported in the experimental study [20], and reduction factors for $E_s(T)$ and $f_y(T)$ were defined in accordance with EN 1993-1-2 [27].

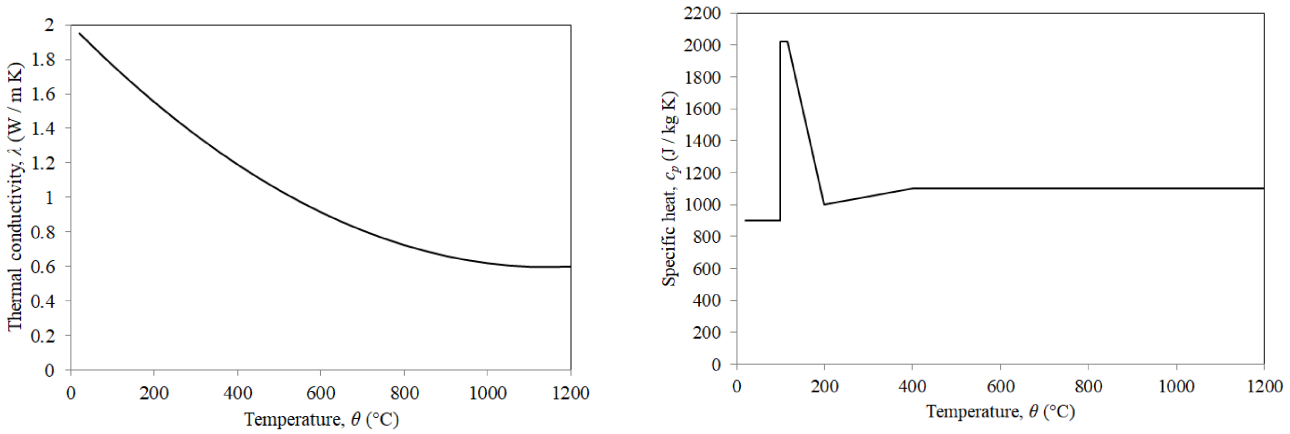

(**a**) (**b**)

Figure 3. Temperature-dependent material properties of concrete according to EN 1992-1-2 [26]: (**a**) thermal conductivity; (**b**) specific heat.

The thermal behavior of steel was also included in the transient analysis using the heat conduction equation:

$$\rho_s(T)c_s(T)\frac{dT}{dt} = \nabla.(k_s(T)\nabla T) \quad (5)$$

where $c_s(T)$ and $k_s(T)$ are the temperature-dependent specific heat capacity and thermal conductivity of steel. The corresponding temperature-dependent relationships are presented in Figure 4.

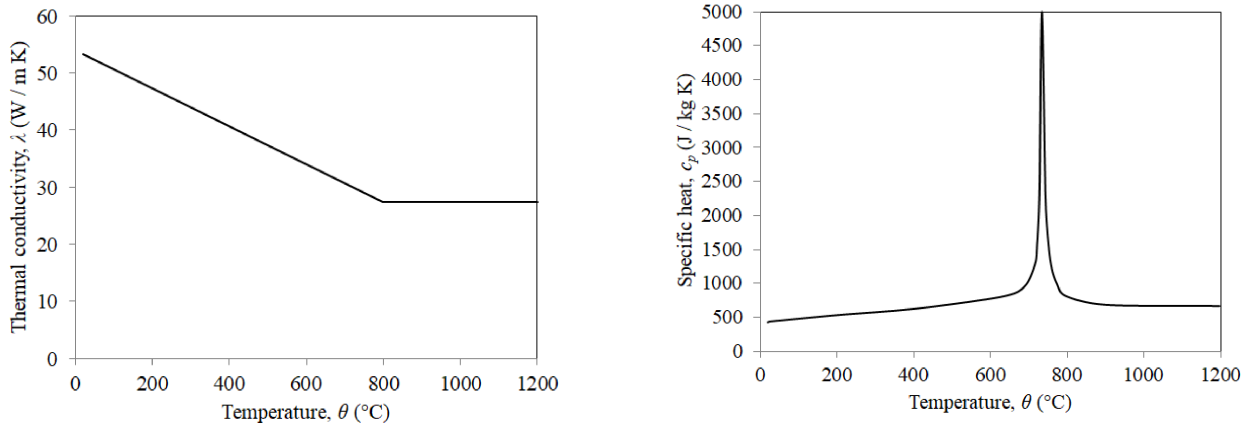

(**a**) (**b**)

Figure 4. Temperature-dependent material properties of reinforcement according to EN 1993-1-2 [27]: (**a**) thermal conductivity; (**b**) specific heat.

To simulate the fire exposure, combined convective and radiative heat transfer mechanisms were considered in the transient thermal analysis. The heat transfer coefficient of concrete (α_c) is defined as 25 W/m^{2}K and the emissivity (ε_m) as 0.7 were adopted in line with EN 1991-1-2 [28]. The temperature history obtained from the thermal analysis was subsequently used to define the degradation of material properties in the structural model, representing the effects of fire exposure on the residual mechanical response.

2.3. Boundary Conditions and Loading

The boundary conditions were defined to replicate the experimental setup reported by Al-Gasham et al. [20], in which two opposite edges were simply supported while the

remaining edges were unrestrained. This configuration was adopted to ensure a direct and consistent comparison between the FE model and the experimental results. The supports were modeled along the top surface as lines parallel to the short edge of the slab, positioned 25 mm inward from each longitudinal end. One edge was defined as simply supported by restraining vertical and transverse displacements, while the opposite edge was modeled as a roller support by restraining only the vertical displacement.

To simulate a simplified thermal exposure and the subsequent structural response, a sequentially coupled thermal–structural analysis was performed in ANSYS Workbench. In the validation stage, a uniform temperature of 800 °C was applied to all slab surfaces for 3600 s (1 h), consistent with the experimental program of Al-Gasham et al. [20], to ensure direct comparability. As the experimental setup does not explicitly define one-sided fire exposure, this uniform heating was adopted as a simplified representation, although it does not fully reflect realistic fire conditions. In contrast, the parametric study considers bottom-surface fire exposure based on the ISO 834 curve, representing a more realistic scenario for slab systems.

The transient thermal results were used to determine the maximum temperature attained at each FE during the heating phase. These temperatures were subsequently used to define the residual degradation of material properties on an element-wise basis in the structural analysis. The structural analysis was then carried out under ambient conditions, assuming that the slab had fully cooled to room temperature.

Importantly, the temperature field obtained from the thermal analysis was not applied as a thermal load in the structural analysis; rather, it was used solely to define temperature-dependent material degradation. Accordingly, thermal strains and thermal expansion effects were not included in the structural model. Since the analysis was performed under a uniform ambient temperature field after cooling, no temperature gradients existed within the slab during the mechanical analysis, and therefore thermally induced curvature (thermal bowing) did not occur.

This approach differs fundamentally from hot-state thermo-mechanical analysis, in which temperature fields are directly applied as thermal loads and thermal strains govern the structural response during fire exposure. The adopted framework therefore represents a simplified post-fire residual structural assessment, focusing on stiffness degradation due to irreversible thermal damage.

In the static structural stage, the mechanical loading was defined in accordance with the experimental procedure reported by Al-Gasham et al. [20]. A uniformly distributed surface load was applied on the bottom face of the slab and acted in the upward direction, representing the load-transfer mechanism used in the experimental setup. The load was applied monotonically in incremental steps of 2.5 kN, consistent with the loading protocol adopted in the reference study. The analysis was continued until a clear loss of stiffness and convergence difficulties were observed, which was taken to indicate the ultimate load capacity of the slab.

2.4. Results and Discussion

Thermal Analysis: In the first stage, a transient thermal analysis was performed for a duration of 60 min to simulate fire exposure at 500 °C and 800 °C. The resulting temperature distributions across the slab thickness are presented in Figure 5. As shown in Figure 5a,b, elevated temperatures are concentrated near the fire-exposed surfaces, while significantly lower temperatures are maintained within the core region, indicating non-uniform heat penetration through the slab thickness. This through-thickness gradient became more pronounced at higher exposure temperature (800 °C), resulting in a wider temperature range between the surface and the slab core.

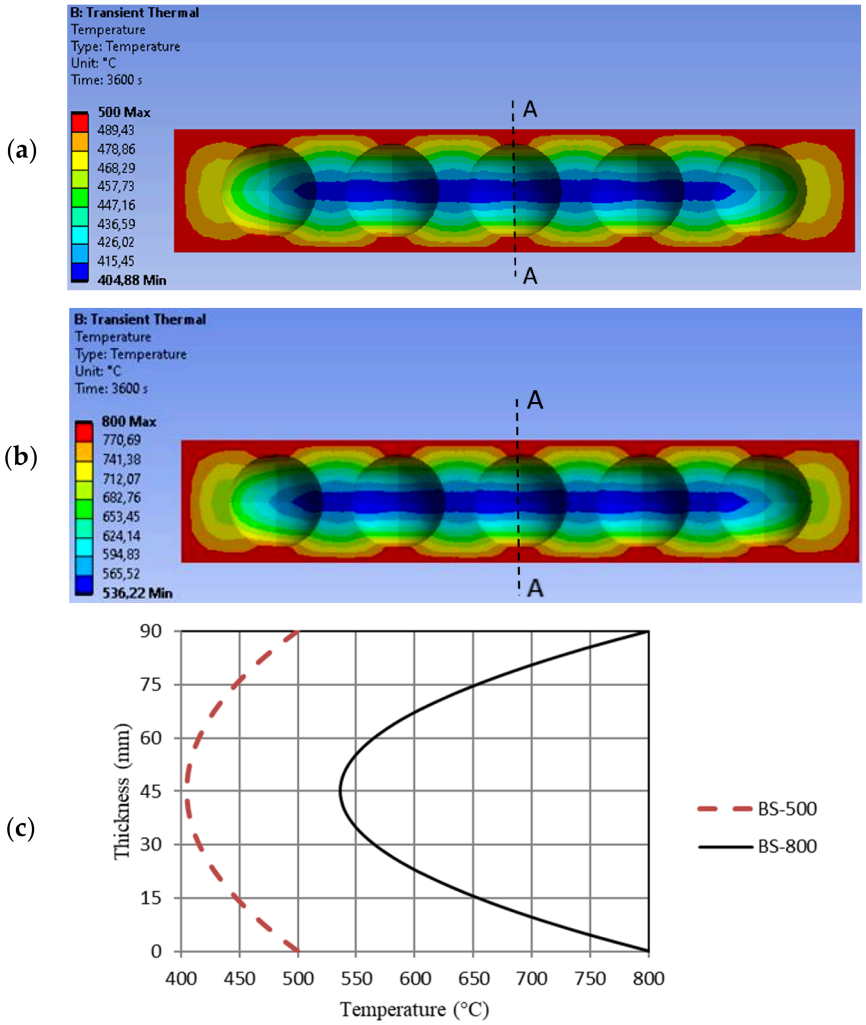

Figure 5. FE-predicted temperature contours for (**a**) BS-500 and (**b**) BS-800, together with (**c**) the corresponding through-thickness temperature profiles along section A–A after 1 h of fire exposure.

The presence of internal voids introduces localized variations in the temperature field, particularly around the void boundaries, where heat transfer paths are altered. Despite these localized effects, the overall temperature distribution exhibits a consistent trend, with temperature decreasing progressively from the exposed surfaces toward the mid-depth of the slab. The through-thickness temperature profiles extracted along section A–A (Figure 5c) further confirm this behavior, showing a nonlinear gradient characterized by steep temperature changes near the exposed surfaces and a relatively stable temperature region toward the slab core. This distribution can be attributed to the relatively low thermal conductivity of concrete combined with the insulating effect of the internal cavities.

Structural Analysis: In the subsequent stage, the maximum temperature attained at each FE during the transient thermal analysis was used to define the corresponding residual degradation of material properties within the structural model, and a nonlinear analysis was performed under ambient conditions. The resulting load–deflection responses are presented in Figure 6 and compared with the experimental results reported by Al-Gasham et al. [20].

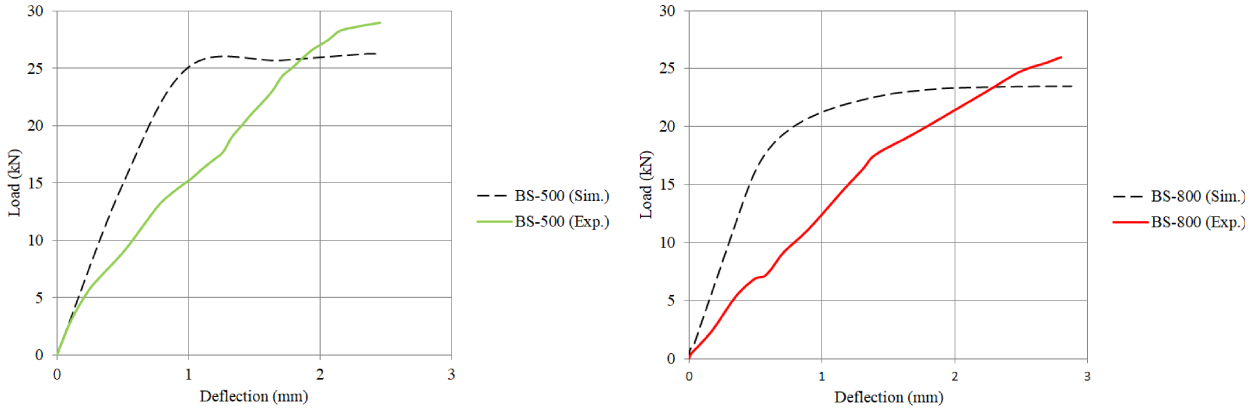

(**a**) (**b**)

Figure 6. Load–deflection curve of slabs: (**a**) BS-500 specimen; (**b**) BS-800 specimen.

As shown in Figure 6, the FE predictions exhibit a slightly stiffer response in the initial loading stage, particularly within the first 1 mm of deflection. This difference can be attributed to modeling idealizations, such as the assumption of perfect support conditions, the absence of initial geometric imperfections, and the simplified representation of material nonlinearity. Despite this, the overall nonlinear response is well captured, and good agreement was observed in terms of ultimate load capacity.

Table 1 summarizes the comparison between experimental and numerical results. The FE model slightly underestimated the ultimate load for both specimens, with differences of 9.48% for BS-500 and 9.65% for BS-800. The corresponding midspan deflections show close agreement, with deviations of 2.80% and 3.57%, respectively. These results indicate that the proposed model provides a reliable and conservative prediction of the residual strength and deformation behavior of fire-exposed slabs. This relatively stiffer response is consistent with the limitations of the adopted modeling framework discussed in Section 2, particularly regarding the representation of cracking-induced stiffness degradation at low stress levels.

Table 1. Comparison between experimental [20] and current FE analysis results.

Specimen	Experiment [20]		FE Analysis		% Difference in Load	% Difference in Displacement
	V_u * (kN)	δ_{ul} (mm)	V_{uc} (kN)	δ_{ulc} (mm)		
BS-500	29.00	2.50	26.25	2.43	9.48	2.80
BS-800	26.00	2.80	23.49	2.90	9.65	3.57

* V_u = Experimental ultimate load, δ_{ul} = Experimental displacement, V_{uc} = Ultimate load calculated, δ_{ulc} = Displacement calculated.

Overall, the agreement between experimental and numerical results confirms that the proposed FE model is capable of capturing the residual structural behavior of fire-exposed voided slabs and is suitable for subsequent parametric investigations, particularly for comparative evaluations based on deflection response.

3. Parametric Study

Following the validation study, the validated FE model was subsequently extended to investigate the residual behavior of full-scale slabs after standard fire exposure and assumed cooling to ambient conditions. To investigate the influence of void geometry on the structural performance of biaxial voided RC slabs after fire exposure, a series of numerical models were developed using the validated FE framework described in Section 2.

The parametric study considers several void geometries while maintaining identical slab dimensions, reinforcement layout, material properties, and boundary conditions. This approach ensures that any variation in structural behavior can be attributed solely to the geometry of the internal voids. Thus, the influence of void geometry on structural performance after fire exposure can be systematically evaluated.

The parametric models include five different void geometries, namely spherical, elliptical, ellipsoidal, capsule, and biaxial capsule, as illustrated in Figure 7. While spherical voids are commonly adopted in practical applications of biaxial voided slab systems, the remaining geometries were generated in this study to assess the influence of void shape on the structural response of the slabs after fire exposure. These configurations are compared with two conventional solid RC slabs.

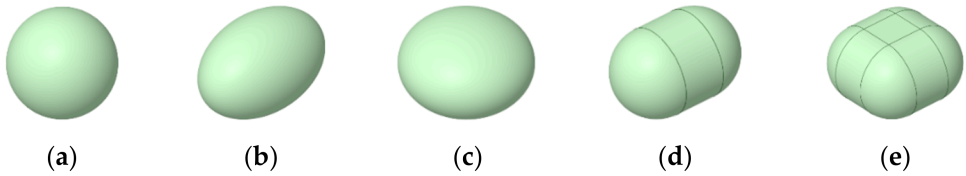

Figure 7. Void shapes considered in the parametric study: (**a**) spherical; (**b**) elliptical; (**c**) ellipsoidal; (**d**) capsule; (**e**) biaxial capsule.

The base design of the parametric study was established in accordance with the BubbleDeck design guideline [29]. Slab models had identical plan dimensions of 4000 × 4000 mm, with all edges simply supported. A slab thickness of 230 mm and a spherical void diameter of 180 mm were selected based on the minimum values specified in [29] as shown in draft Figure 8. The remaining void geometries were defined with reference to the spherical configuration while maintaining an equivalent total concrete volume across all models.

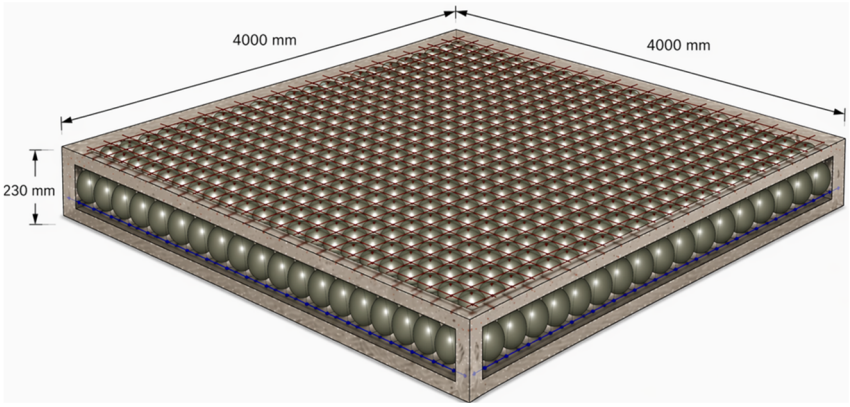

Figure 8. Three-dimensional view of the biaxial voided RC slab with internal spherical voids and orthogonal reinforcement layers.

The reinforcement layout, including bar diameters, spacing, and concrete cover, was also defined in accordance with the same guideline and kept identical for all slab configurations, including solid slabs, to ensure a consistent basis for comparison. Each slab was reinforced with 8 mm diameter bars in the top layer and 10 mm diameter bars in the bottom layer, arranged at 200 mm spacing in both directions, with a concrete cover of 20 mm.

The applied loading consisted of the self-weight of the slab and a uniformly distributed load of 5 kN/m^2, defined in accordance with EN 1991-1-1 [30], representing typical service-level loading conditions.

This dual comparison approach enables the influence of void geometry to be evaluated from two complementary perspectives: (i) structural response under identical thickness conditions (230 mm for both solid and voided slabs), where the corresponding concrete volumes are approximately 3.7 m^3 and 2.6 m^3, respectively; and (ii) performance under equivalent concrete volume (2.6 m^3), where the solid and voided slabs have thicknesses of 160 mm and 230 mm, respectively. Accordingly, the effect of void geometry can be distinguished from purely geometric stiffness differences, allowing for a more rigorous assessment of the structural performance of voided slab systems.

3.1. Geometry, Slab Configurations, and FE Mesh

The geometric parameters of the voids are presented in Figure 9. The reinforcement layout is shown in Figure 10, while Figure 11 illustrates the one-quarter slab models adopted in the numerical analysis using geometric and loading symmetry.

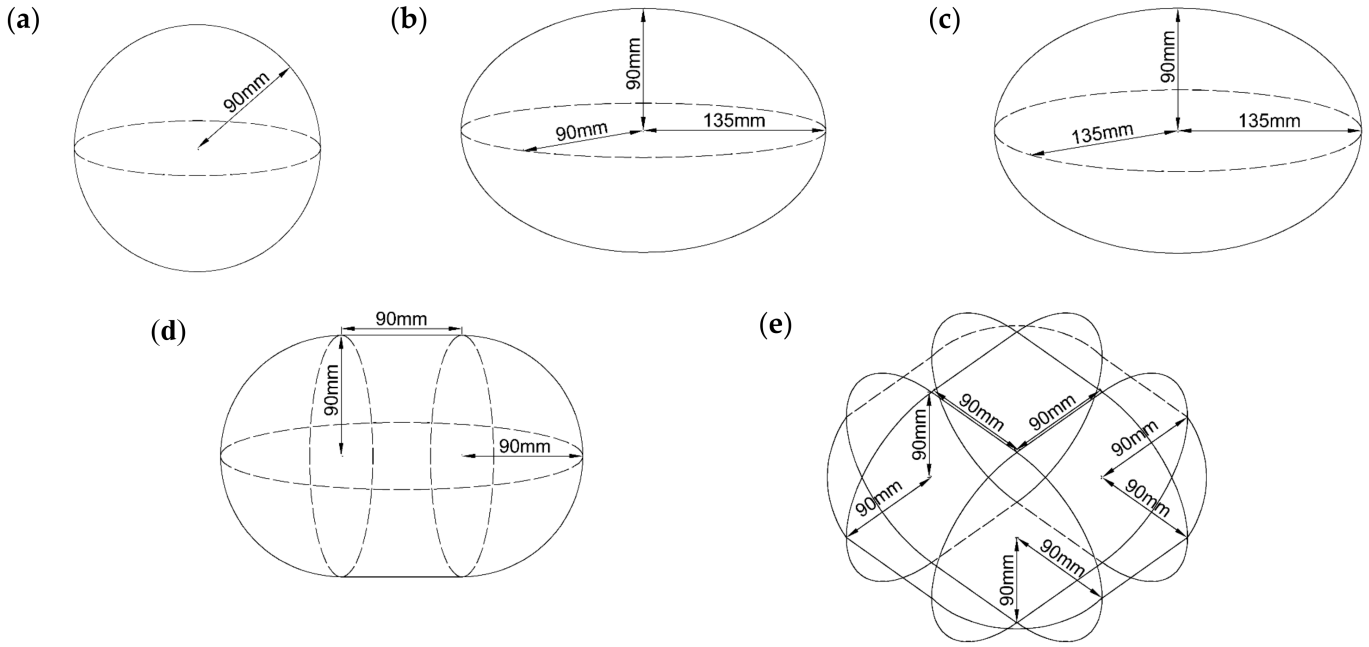

Figure 9. Geometry and dimensions of the void shapes: (**a**) spherical; (**b**) elliptical; (**c**) ellipsoidal; (**d**) capsule; (**e**) biaxial capsule.

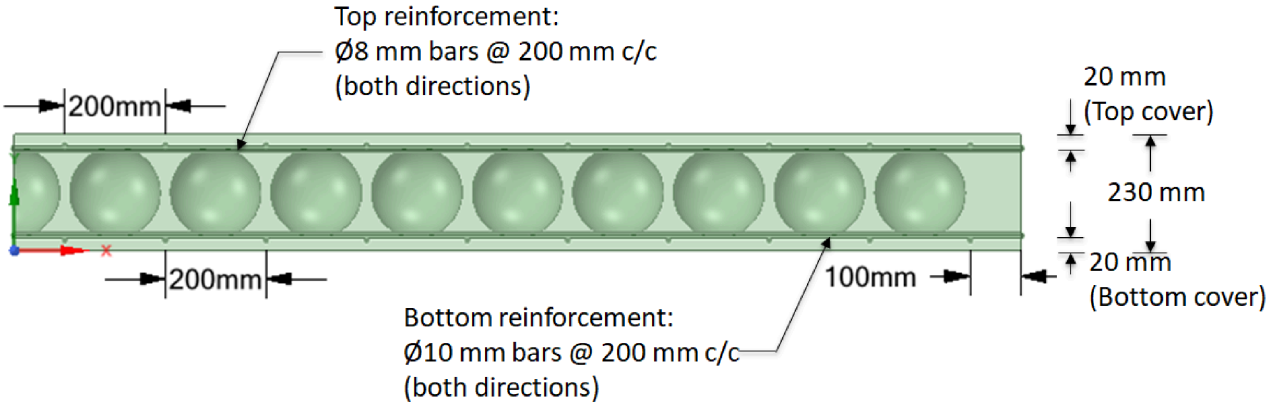

Figure 10. Half of the cross-sectional view of the biaxial voided RC slab showing spherical voids, reinforcement layout details.

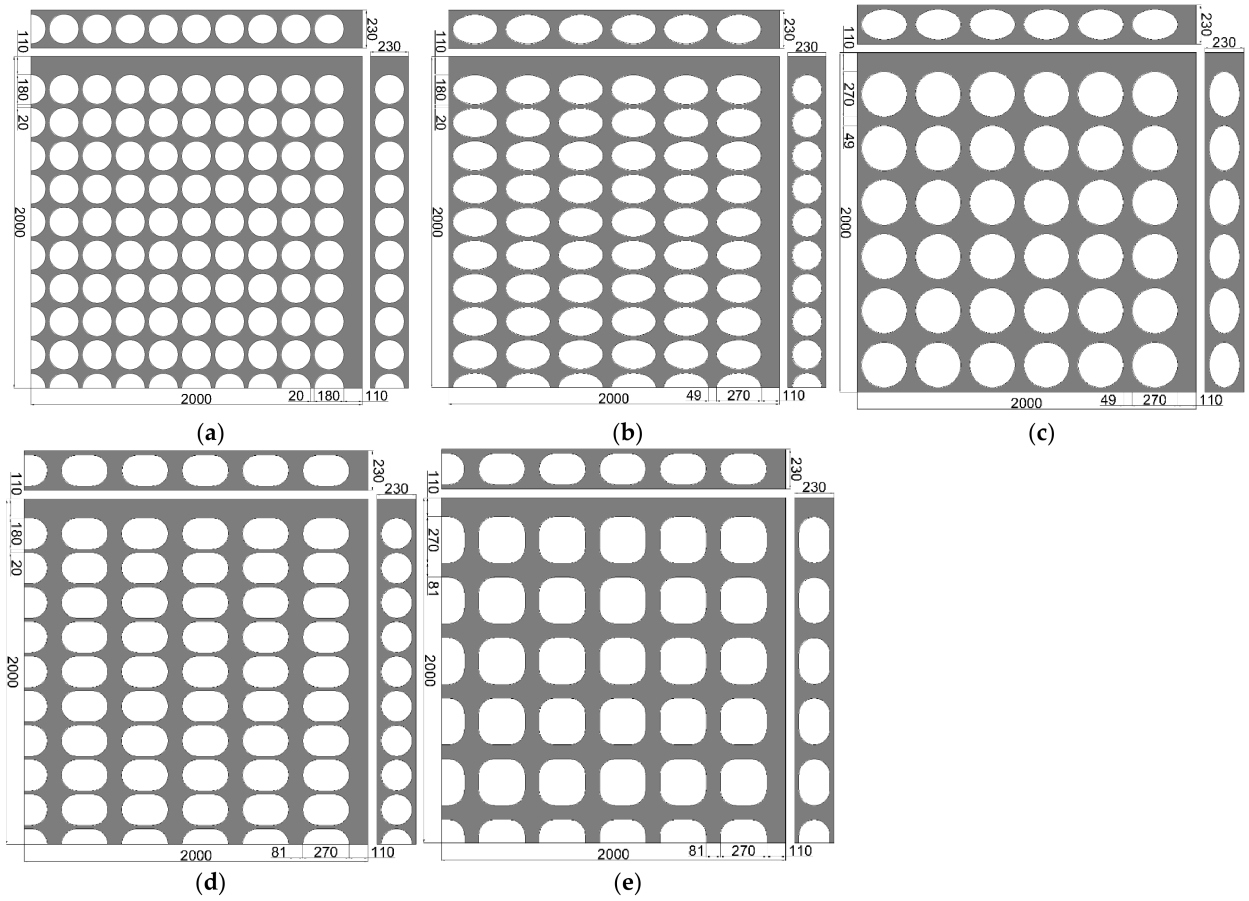

Figure 11. Plan and cross-sectional views of RC slab models (all dimensions in mm): (**a**) spherical; (**b**) elliptical; (**c**) ellipsoidal; (**d**) capsule; (**e**) biaxial capsule.

The voids were arranged in a regular grid pattern within the slab plan, while maintaining sufficient concrete regions between adjacent voids and near the slab edges. The spacing and edge distances of the voids were defined in accordance with the recommendations provided in the BubbleDeck design guideline [29], originally developed for spherical void systems. This configuration ensures adequate concrete webs for effective load transfer and reinforcement placement while maintaining practical constructability.

The meshing strategy adopted in the parametric models was based on the validated numerical model described in Section 2 and further refined through preliminary numerical trials involving different mesh densities. Several element sizes were evaluated to examine their influence on numerical stability and the global structural response. It was observed that further mesh refinement beyond a certain threshold did not result in a significant change in key response parameters, while considerably increasing computational cost.

Accordingly, a structured mesh composed predominantly of hexahedral elements was employed, as shown in Figure 12. The maximum element size was selected as approximately 38 mm for the voided slab models and 40 mm for the solid slab models, providing an appropriate balance between computational efficiency and solution accuracy. This meshing strategy is consistent with the approach reported by Miller et al. [23] for similar voided slab systems subjected to fire conditions.

The steel reinforcement was modeled using embedded line elements with a compatible mesh density to ensure proper interaction with the surrounding concrete.

Due to the adopted void diameter of 180 mm within a 230 mm thick slab, the remaining concrete cover is approximately 25 mm. While the selected mesh size provides sufficient accuracy for global response parameters, the resolution of highly localized thermal gradients

within this thin region is inherently limited. However, this does not affect the comparative conclusions of the study, as the overall structural response is primarily governed by the through-thickness temperature distribution and corresponding material degradation, as also supported by the validation results.

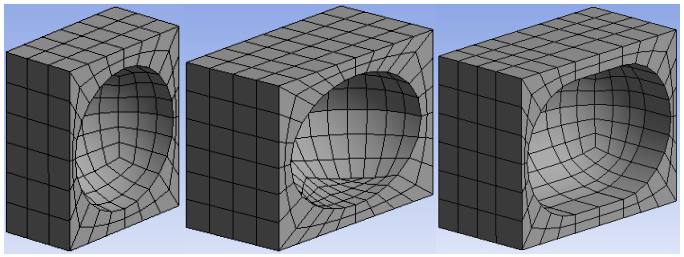

Figure 12. FE mesh of the voids: (**a**) spherical; (**b**) elliptical/ellipsoidal; (**c**) capsule/biaxial capsule.

3.2. Material Modeling

The material models adopted in the parametric study are consistent with those defined in the validation stage (Section 2.1). Concrete was modeled as C30, while the reinforcement was defined as S500 grade steel. The temperature-dependent degradation of mechanical properties for both materials was implemented in accordance with EN 1992-1-2 [26] for concrete and EN 1993-1-2 [27] for reinforcing steel. The corresponding reduction relationships are presented in Figure 13.

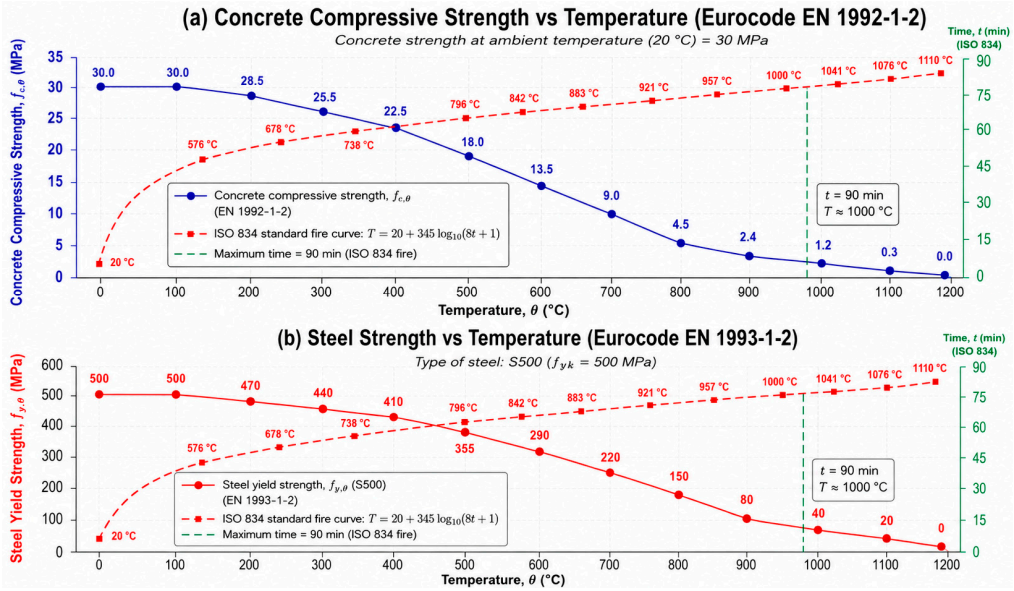

Figure 13. Temperature-dependent degradation of material strength according to Eurocodes: (**a**) concrete compressive strength based on EN 1992-1-2; (**b**) reinforcing steel yield strength based on EN 1993-1-2 under ISO 834 standard fire exposure.

3.3. Boundary Conditions and Loading

The parametric analyses were performed using the same sequential thermal–structural framework described in Section 2.3, in which the temperature field is used solely to define residual material degradation, and the structural response is evaluated under ambient conditions after assumed cooling.

In the parametric study, all slab models were assumed to be simply supported along their four edges. This idealized boundary condition was selected to provide a consistent and symmetric structural system, enabling a clear comparison of the influence of void

geometry. While fully restrained conditions may better represent in-situ slab–beam systems, the adopted approach isolates the effect of geometric parameters and ensures compatibility with the validation framework.

The applied mechanical loads included the self-weight of the slab and a uniformly distributed design load of 5 kN/m^2, representing typical floor loading conditions. The magnitude of this load was determined in accordance with EN 1991-1-1 [30], corresponding to the upper range of imposed loads for public and commercial buildings. This value was selected to provide a conservative assessment of structural performance under service conditions. Partial safety factors were not applied, as the analysis focuses on residual structural response rather than design verification.

Geometric and loading symmetry was utilized, and only one-quarter of the slab was modeled in the numerical simulations. Along the symmetry planes, displacement normal to the symmetry surface was constrained. The loading and symmetry boundary conditions are illustrated in Figure 14. In this figure, edges A and B represent the symmetry planes, while edges C and D correspond to the simply supported boundaries. The uniformly distributed load is indicated by label E, acting downward on the slab surface.

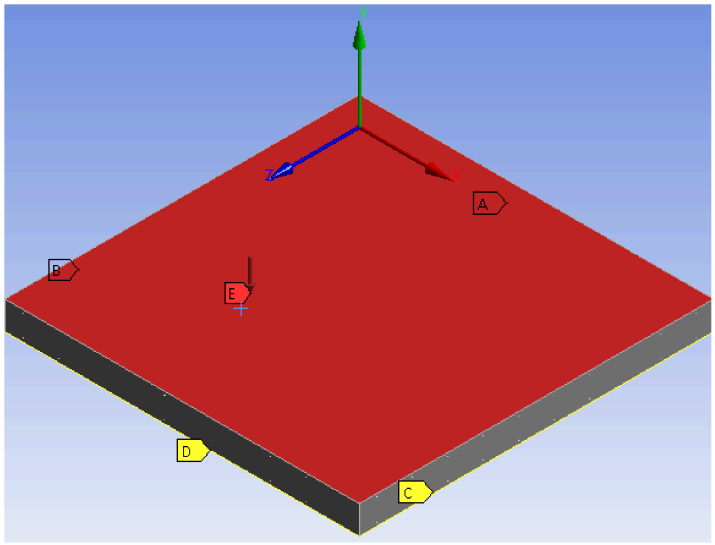

Figure 14. Loading and symmetry boundary conditions.

In fire engineering, different fire curves are selected depending on the fire scenario. The ISO 834 used in this study represents a typical cellulosic fire and is widely adopted for structural fire resistance assessment due to its simplicity and standardization. However, alternative curves exist for different conditions. For example, ASTM E119 provides a similar standard exposure, while hydrocarbon fire curves exhibit a much more rapid temperature rise and higher peak temperatures (~1100 °C), making them suitable for petrochemical applications. Tunnel fire curves (e.g., RWS, RABT) represent extreme confined fires with peak temperatures up to 1350 °C. In contrast, parametric fire models defined in EN 1991-1-2 account for ventilation, fire load, and compartment properties, and include both heating and cooling phases, providing a more realistic representation of natural fire behavior [31].

It should be noted that the ISO 834 curve represents a continuously increasing temperature profile and does not include a cooling phase. In real fire scenarios, temperatures typically increase to a peak value and subsequently decrease during cooling, which may influence the residual structural response through thermal gradients and stress redistribution. Therefore, while the present study provides a consistent basis for comparative evaluation, the structural response under natural fire conditions may differ.

Fire exposure was applied to the bottom surface of the slab, representing a typical floor system subjected to fire from the compartment below. The thermal boundary condition followed the ISO 834 standard fire curve [24], defined as:

$$T(t) = 20 + 345\, log_{10}(8t + 1) \quad (6)$$

where $T(t)$ is the temperature in °C and t is the time in minutes.

The fire exposure durations considered were 30, 60, and 90 min, representing increasing levels of thermal damage. For each case, a transient thermal analysis was performed to determine the temperature distribution within the slab. The maximum temperature attained at each FE during the heating phase was then used to assign temperature-dependent residual material properties on an element-wise basis. The subsequent structural analysis was carried out under ambient conditions, assuming that the slab had fully cooled to room temperature. Accordingly, the reported structural response represents residual behavior governed by stiffness degradation due to irreversible thermal damage.

Load-induced thermal strain (LITS) is not considered in the present study. LITS develops when mechanical loading is applied simultaneously with increasing temperature during fire exposure. In the adopted modeling approach, the structural analysis is performed after completion of the thermal phase under ambient conditions, assuming that the slab has cooled and only residual material degradation remains. As a result, transient thermo-mechanical interactions during heating, including LITS, are not captured. This modeling approach is consistent with a simplified post-fire residual assessment framework and is intended to evaluate the remaining structural capacity rather than the deformation response during the heating phase.

4. Results and Discussion

4.1. Temperature Distribution After Fire

According to the ISO 834 standard fire curve [24], the gas temperatures corresponding to fire exposure durations of 30, 60, and 90 min are approximately 842 °C, 945 °C, and 1006 °C, respectively, as shown in Figure 13. While the temperature increases rapidly during the initial stages of fire exposure, the rate of increase gradually decreases with time.

Since the concrete cover was kept constant at 20 mm for all configurations, the observed differences in temperature distribution can be attributed primarily to the void geometry and the resulting changes in local heat transfer paths.

The results indicated that heat penetration within both solid and voided slabs is governed primarily by the duration of fire exposure rather than the absolute temperature level. As the exposure time increases, heat progressively penetrates deeper into the slab thickness, resulting in a gradual rise in temperature within the core region. After 30 min of fire exposure, elevated temperatures are largely confined to the lower portion of the slab. At 60 min, heat penetration becomes more pronounced, extending further toward the mid-depth. By 90 min, a significant portion of the slab thickness is affected, indicating substantial thermal influence throughout the section.

4.1.1. Solid Slabs

The temperature distribution within the solid slab after 30, 60, and 90 min of fire exposure is presented in Figure 15. As expected, elevated temperatures are concentrated near the fire-exposed bottom surface, while significantly lower temperatures are observed toward the upper regions of the slab. This results in the formation of a pronounced temperature gradient across the slab thickness, which becomes increasingly pronounced with longer fire exposure durations.

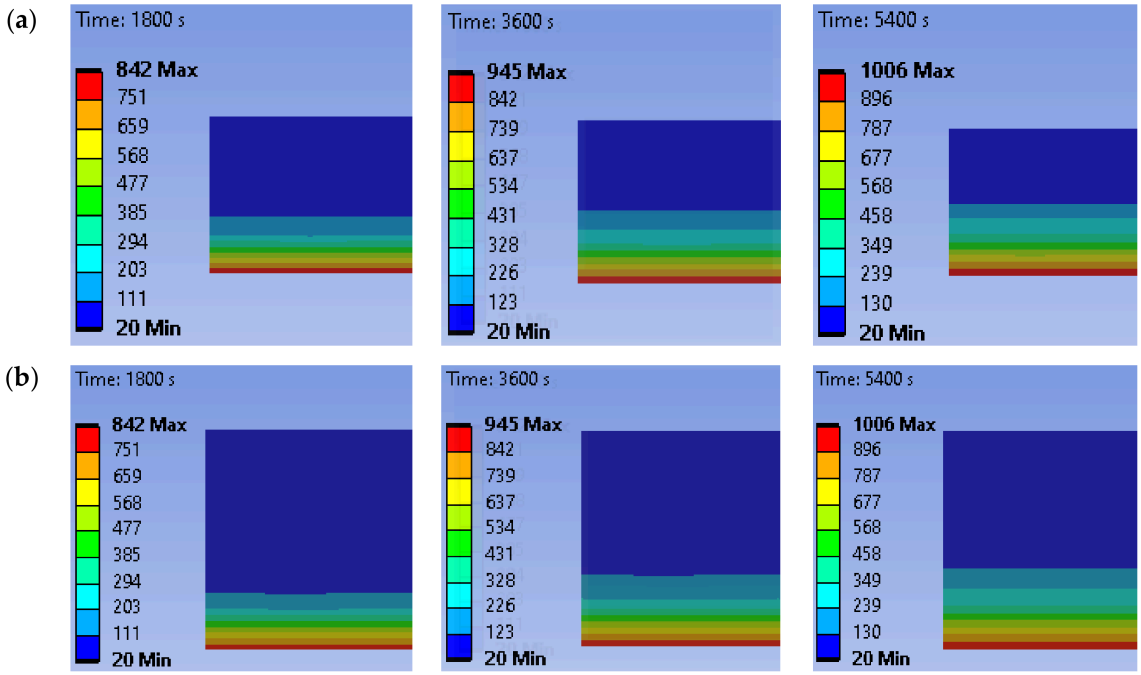

Figure 15. Temperature profile of solid slabs after 30, 60, and 90 min of fire exposure: (**a**) Solid160; (**b**) Solid230.

To further assess the accuracy of the numerical model, the temperature distribution obtained from the FE analysis was compared with the temperature profiles specified in Eurocode 2 for solid slabs [26]. This comparison was carried out using the 160 mm thick solid slab, as presented in Figure 16, to provide a consistent reference case for model verification.

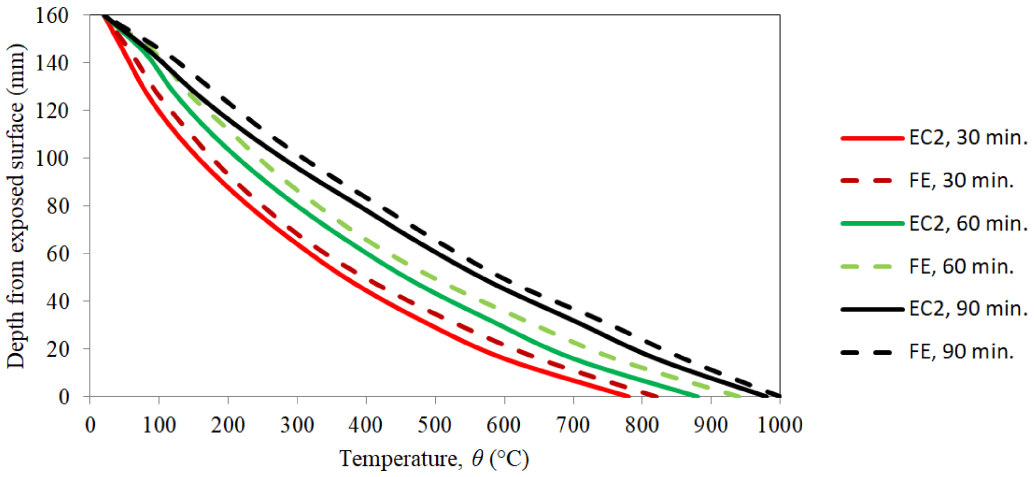

Figure 16. Comparison of temperature distributions for the solid slab based on EN 1992-1-2 [26].

The comparison demonstrates good agreement in terms of the overall temperature gradient and distribution trend across the slab thickness. A slight discrepancy is observed, with the FE model predicting marginally higher temperatures at intermediate depths. This difference can be attributed to the fact that the Eurocode temperature profiles are based on generalized one-dimensional reference conditions, whereas the present FE model reflects the specific geometry and boundary conditions of the slab, including heat transfer characteristics associated with finite thickness.

Despite these minor differences, the overall agreement confirms that the developed FE model is capable of accurately capturing the through-thickness temperature distribution of RC slabs under standard fire exposure conditions.

4.1.2. Voided Slabs

Following the analysis of the solid slabs, the temperature distribution in voided slab configurations is examined to evaluate the influence of internal voids on heat transfer. Figure 17 presents the temperature distribution within the spherical voided slab for different fire exposure durations. Similar to the solid slabs, elevated temperatures are concentrated near the fire-exposed bottom surface, while a pronounced temperature gradient develops through the slab thickness.

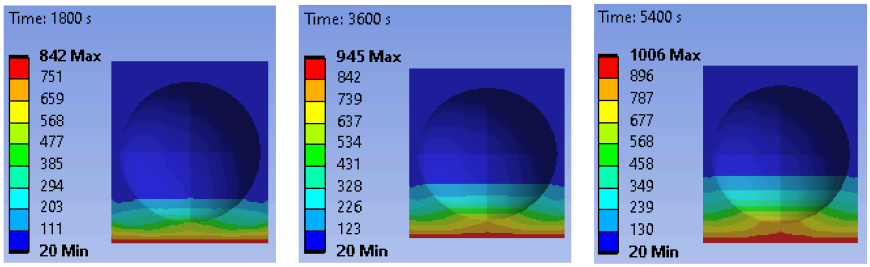

Figure 17. Temperature profile of the spherical slab after 30, 60, and 90 min of fire exposure.

The presence of internal voids introduces localized thermal gradients, particularly around the void boundaries, where heat transfer paths are altered. These localized effects are more evident at early stages of fire exposure (e.g., 30 min), indicating rapid temperature variation in the vicinity of the voids. However, despite these local variations, the overall through-thickness temperature gradient remains comparable to that of the solid slabs, suggesting that the global thermal response is not significantly affected by the presence of voids.

As the exposure time increases, differences between configurations became more pronounced, particularly at 90 min, due to deeper heat penetration. Therefore, the comparison is primarily focused on the 90 min exposure, where the influence of void geometry can be more clearly distinguished, as shown in Figure 18.

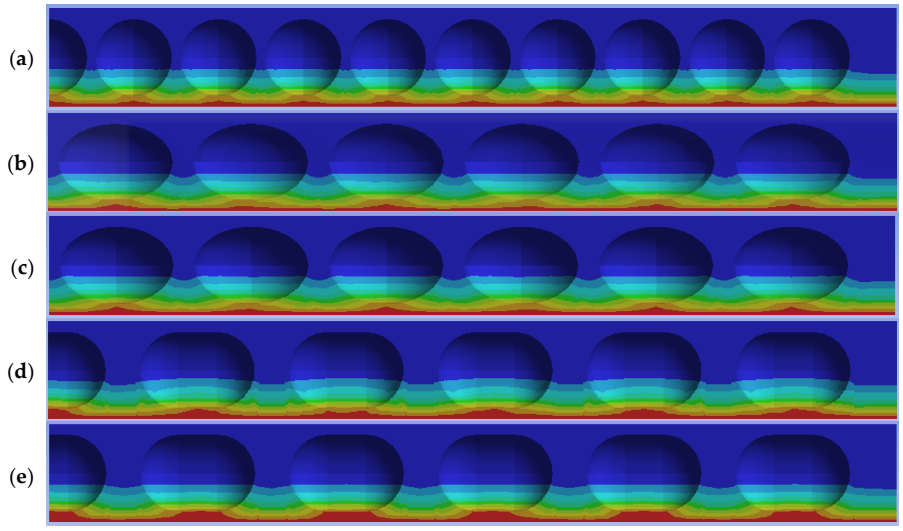

Figure 18. Temperature distributions of slabs with different void geometries after 90 min: (**a**) spherical; (**b**) elliptical; (**c**) ellipsoidal; (**d**) capsule; (**e**) biaxial capsule.

Although the overall temperature gradient remains broadly consistent across all configurations, localized variations are observed depending on the void shape. The ellipsoidal geometry exhibited a more uniform and continuous temperature distribution, while the spherical configuration shows a relatively regular pattern. In contrast, the biaxial capsule geometry resulted in more pronounced localized temperature concentrations, with a larger portion of the lower region reaching higher temperatures.

To further quantify these observations, through-thickness temperature profiles at the slab midspan were extracted for all void configurations at 30, 60, and 90 min of fire exposure, as presented in Figure 19. The results show that temperature decreases significantly with increasing distance from the fire-exposed surface. A steep thermal gradient is observed near the bottom surface, while beyond approximately 120 mm depth (up to the top surface at 230 mm), the temperature remains close to ambient for all cases.

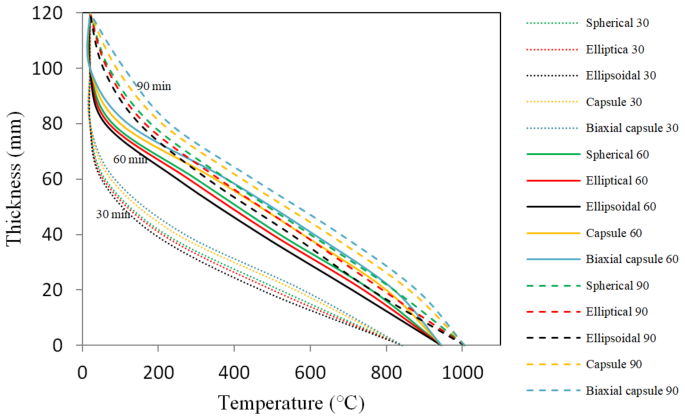

Figure 19. Transient temperature profiles at the slab midspan for different void configurations after 30, 60, and 90 min of fire exposure, showing the temperature variation from the fire-exposed bottom surface to 120 mm depth of slabs, beyond which temperatures remain close to ambient conditions.

The influence of void geometry on thermal response is primarily local rather than global. Although all slab configurations exhibit a similar overall through-thickness temperature gradient, the geometry of the void alters the local heat-flow path around the cavity. Geometries with smoother and more continuous curvature, such as the ellipsoidal void, promote a more gradual temperature transition around the void boundary. In contrast, capsule-type and biaxial capsule voids create wider heated regions near the lower part of the slab, leading to more pronounced localized thermal concentrations. As a result, the thermal field remains broadly similar at the slab scale, while the local distribution near the void boundaries becomes geometry-dependent, particularly after prolonged exposure.

4.2. Structural Response After Fire

The residual structural response of the slabs after fire exposure and assumed cooling is characterized through midspan deflection. The deformation patterns of representative slab configurations at 90 min of fire exposure are illustrated in Figure 20, where the differences between slab configurations become more pronounced.

Table 2 summarizes the midspan deflections at ambient conditions and after 30, 60, and 90 min of fire exposure. The results showed a consistent increase in deflection with increasing fire duration for all slab types, indicating progressive stiffness degradation due to thermal exposure. The relatively small absolute deflection values reported in Table 2 are consistent with the modeling characteristics discussed in Section 2, where cracking-induced stiffness degradation is not fully represented at service-level loading. Accordingly, the results remain reliable for comparative evaluation of structural performance, which constitutes the primary objective of this study, rather than for absolute serviceability prediction.

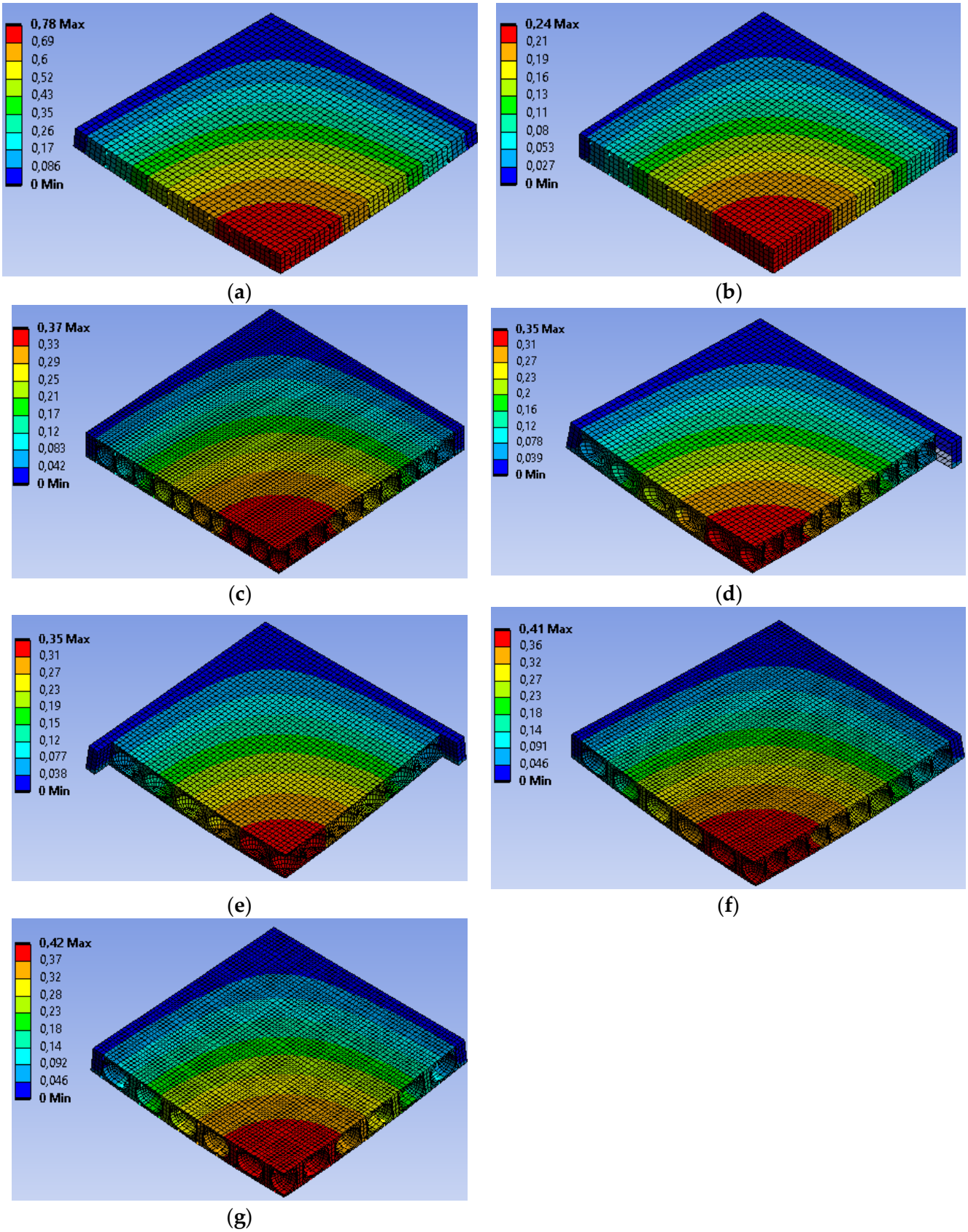

Figure 20. Deformation patterns of slab configurations after 90 min of fire exposure: (**a**) Solid160; (**b**) Solid230; (**c**) spherical; (**d**) elliptical; (**e**) ellipsoidal; (**f**) capsule; (**g**) biaxial capsule.

Table 2. Midspan deflection values and normalized deflection ratios relative to ambient condition.

	Slab	Thickness (mm)	Volume (m^3)	$\delta_{20°C}$ * (mm)	δ_{30} (mm)	δ_{60} (mm)	δ_{90} (mm)	$\frac{\delta_{30}}{\delta_{20°C}}$	$\frac{\delta_{60}}{\delta_{20°C}}$	$\frac{\delta_{90}}{\delta_{20°C}}$
	Solid160	160	2.6	0.45	0.62	0.71	0.78	1.38	1.58	1.73
	Solid230	230	3.7	0.16	0.20	0.22	0.24	1.25	1.38	1.50
Void	Spherical	230	2.6	0.19	0.25	0.31	0.37	1.32	1.63	1.95
Void	Elliptical	230	2.6	0.18	0.24	0.29	0.35	1.33	1.61	1.94
Void	Ellipsoidal	230	2.6	0.18	0.24	0.29	0.35	1.33	1.61	1.94
Void	Capsule	230	2.6	0.19	0.27	0.34	0.41	1.42	1.79	2.16
Void	Biaxial capsule	230	2.6	0.20	0.28	0.35	0.42	1.40	1.75	2.10

* $\delta_{20°C}$ is the midspan deflection at ambient temperature (before fire start). δ_{30}, δ_{60}, and δ_{90} are the midspan deflections after 30, 60 and 90 min fire respectively.

It should also be noted that the applied service load level (self-weight + 5 kN/m^2) remains significantly below the ultimate load capacity of the slabs, and therefore the structural response is confined to the pre-peak regime.

It should also be noted that, even after 90 min of fire exposure, the upper portion of the slab remains at relatively low temperatures (Figure 19), indicating that a significant part of the cross-section retains its original stiffness. Consequently, the effective flexural rigidity of the slab is only partially reduced, which contributes to the relatively limited increase in deflection.

For solid slabs, the 160 mm thick slab exhibits the highest deflections, increasing from 0.45 mm at ambient conditions to 0.78 mm after 90 min. In contrast, the 230 mm thick slab shows significantly lower deflections, ranging from 0.16 mm to 0.24 mm over the same exposure durations. This difference is primarily attributed to the higher flexural stiffness associated with increased slab thickness.

Voided slabs exhibited lower deflections than the 160 mm solid slab at all stages, reflecting the comparison based on equivalent concrete volume. Their deflections increase from approximately 0.18–0.20 mm at ambient conditions to 0.35–0.42 mm after 90 min. Among the voided configurations, elliptical and ellipsoidal geometries consistently showed the lowest deflections, while capsule and biaxial capsule geometries exhibit relatively higher values.

Although the temperature of the bottom reinforcement is an important parameter influencing flexural performance, it should not be used alone to assess the overall structural behavior. The temperature evolution of the bottom tensile reinforcement for different void geometries is presented in Figure 21. In this context, the lower reinforcement temperature observed in the spherical slab should not be interpreted as superior overall performance, as reinforcement temperature alone does not directly govern the structural response.

The corresponding temperature values of the bottom tensile reinforcement indicate a clear increase with fire exposure duration for all slab configurations. At 30 min, the temperatures remain relatively close, ranging from approximately 492 °C for the elliptical slab to 605 °C for the biaxial capsule configuration. However, as the exposure time increases, the differences become more pronounced. At 60 min, the reinforcement temperature varies between about 624 °C in the spherical slab and 815 °C in the biaxial capsule slab, while at 90 min it ranges from approximately 714 °C to 920 °C. Among the configurations, the spherical slab consistently exhibits lower reinforcement temperatures, whereas capsule and biaxial capsule geometries result in significantly higher values due to increased heat concentration in the lower region of the slab.

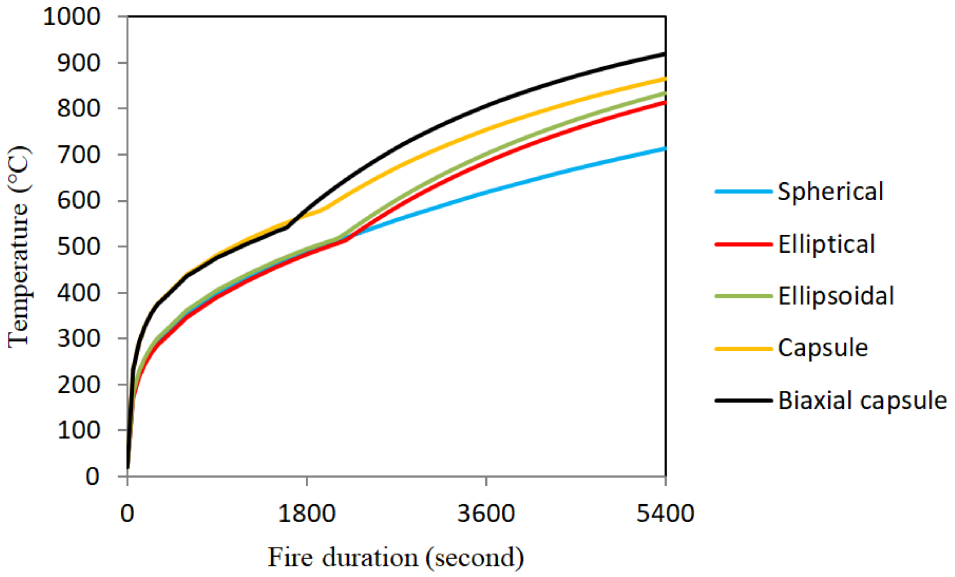

Figure 21. Temperature evolution of bottom reinforcement for different void geometries under ISO 834 fire exposure.

Despite these differences in reinforcement temperature, the global structural response is not governed by steel temperature alone but by the combined effects of material degradation and section stiffness. In this context, when compared with the 230 mm solid slab, all voided slabs exhibit higher deflections due to reduced effective stiffness caused by the presence of internal voids. This highlights the distinction between material efficiency and geometric stiffness: voided slabs perform favorably relative to the 160 mm slab but remain less stiff than the solid slab of identical thickness.

The normalized deflection ratios with respect to ambient conditions further clarify the structural behavior. For the solid slabs, the 160 mm thick slab exhibits ratios increasing from 1.38 at 30 min to 1.73 at 90 min, while the 230 mm thick slab shows a comparatively lower increase, from 1.25 to 1.50 over the same exposure durations.

For the voided slabs, the normalized deflection ratios range from 1.32–1.42 at 30 min, 1.61–1.79 at 60 min, and 1.94–2.16 at 90 min, indicating a more pronounced relative increase in deformation at later stages of fire exposure.

A two-stage response can be identified. During the initial phase (up to 30 min), voided slabs exhibit a comparable or slightly lower rate of stiffness degradation, mainly due to their greater overall depth and limited heat penetration. Beyond this stage, the rate of deformation increases more rapidly, as deeper heat penetration reduces the effective stiffness of the section and diminishes the initial advantage provided by increased depth.

Despite this accelerated degradation at later stages, the absolute deflections of voided slabs remain lower than those of the 160 mm solid slab, while exceeding those of the 230 mm slab. This emphasizes the importance of evaluating structural performance in terms of both geometric stiffness and material efficiency.

Figure 22 presents the residual midspan deflection values obtained after 30, 60, and 90 min of fire exposure. These values correspond to independent post-fire analyses and do not represent a continuous deflection–time response during heating. Among the voided slabs, the biaxial capsule geometry exhibits the highest deflections, while elliptical and ellipsoidal geometries demonstrate relatively more stable behavior.

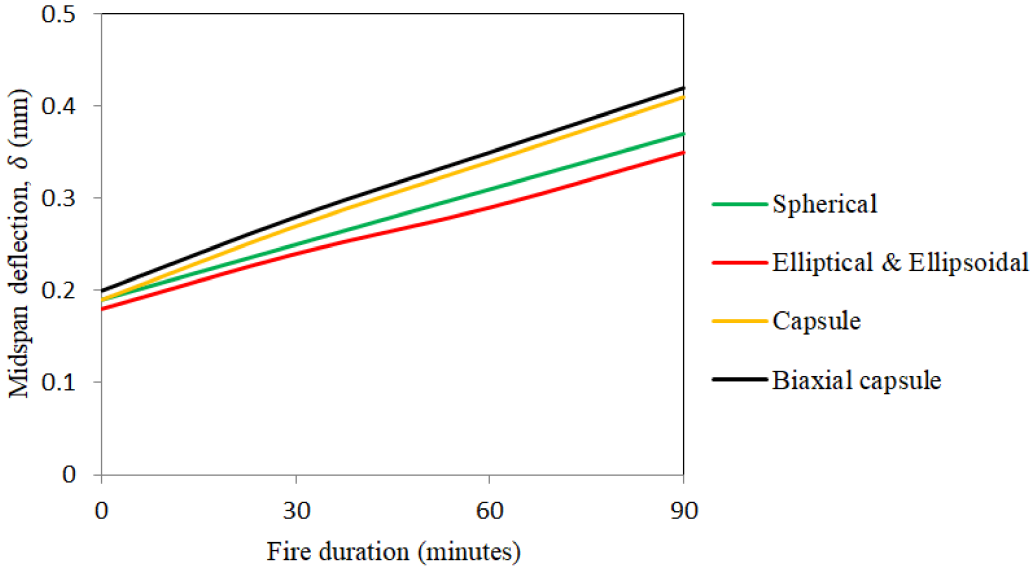

Figure 22. Residual midspan deflection values of slab configurations after 30, 60, and 90 min of ISO 834 fire exposure.

The effect of void geometry on structural response is governed by the combined influence of temperature penetration and effective sectional stiffness. At early fire durations, the thermal effect is largely confined to the lower portion of the slab, and the greater overall depth of the voided slabs helps maintain flexural stiffness. However, as fire duration increases, heat penetrates deeper into the section and the temperature-dependent degradation of concrete and steel becomes more significant. Under these conditions, the internal void layout plays a more important role in governing stiffness loss and stress redistribution. Void shapes such as elliptical and ellipsoidal geometries provide a more uniform concrete distribution around the cavity, which promotes smoother stress transfer and reduces local concentration effects. By contrast, capsule and biaxial capsule configurations lead to less favorable concrete continuity in the heated tension zone, resulting in greater stiffness degradation and larger midspan deflections.

Internal voids may reduce the effective shear-resisting area and alter load-transfer mechanisms in biaxial voided slabs, making shear and punching strength critical, particularly near concentrated-load regions. Previous studies have shown that void layout, concrete web width, and reinforcement detailing significantly influence shear capacity [9,12,13]. However, the present study focuses on residual deformation under service-level loading after fire exposure; therefore, shear strength is not directly evaluated and is identified as a topic for future research.

In voided slab systems, the presence of internal cavities reduces the effective shear-resisting area and concentrates shear stresses within the concrete webs between adjacent voids. Under fire exposure, these regions are particularly vulnerable, as elevated temperatures rapidly reduce concrete tensile strength and shear transfer capacity. Consequently, shear-critical failure modes such as web shear or punching may occur prior to flexural failure, especially under higher load levels or severe thermal degradation.

In the present study, the structural response is evaluated under service-level loading conditions, where the slabs remain within the pre-peak regime and flexural deformation governs the global behavior. Therefore, midspan deflection provides a consistent basis for comparative assessment of different void geometries. However, the results should not be interpreted as a direct indicator of ultimate capacity or failure mode. A detailed evaluation of shear stress distribution and punching resistance under fire conditions is required for comprehensive structural assessment and is recommended for future research.

Explosive spalling is an important phenomenon in fire-exposed RC, driven by pore pressure build-up, moisture migration, and thermal stresses. In voided slabs, internal cavities may influence local heat transfer and moisture movement. However, spalling was not explicitly modeled in this study. Its accurate prediction requires fully coupled hygro-thermo-mechanical analysis, often formulated as a moving boundary problem [32], along with detailed experimental calibration of material properties [33]. Therefore, the present results represent residual structural behavior without accounting for material loss due to spalling.

Advanced nonlinear constitutive formulations have been used in the literature to provide a more detailed representation of material nonlinearity and stiffness degradation in reinforced concrete structures under complex loading conditions [34]. However, the present study focuses on the comparative post-fire residual behavior of biaxial voided slabs under service-level loading conditions using a simplified thermo-structural framework. Therefore, the standard temperature-dependent material formulations available in ANSYS Workbench together with Eurocode-based degradation relationships were considered sufficient for the objectives of the study.

The occurrence of explosive spalling would significantly alter the structural response of voided slabs. Loss of the bottom concrete cover would directly expose the internal void cavities and reinforcement to elevated temperatures, resulting in a more rapid temperature rise in the tensile zone. This would accelerate the degradation of both concrete and steel, reduce the effective cross-sectional depth, and lead to a pronounced decrease in flexural stiffness and load-carrying capacity. Consequently, higher deflections and earlier onset of failure would be expected compared to the present predictions. Therefore, the results should be interpreted with caution in scenarios where significant material loss due to spalling may occur, and the potential influence of spalling should be taken into account in practical fire design.

From a design perspective, the results highlight a fundamental trade-off between stiffness and material efficiency. Voided slabs can achieve comparable deformation performance with reduced concrete volume, particularly at early fire exposure stages. However, their increased sensitivity to stiffness degradation under prolonged fire exposure should be carefully considered in design.

5. Conclusions and Key Findings

This study presented a three-dimensional nonlinear FE investigation of the thermal exposure and simplified post-fire residual structural behavior of RC slabs with different void geometries. The response of solid and voided slab systems was evaluated under ISO 834 standard fire exposure for durations of 30, 60, and 90 min. Two comparison approaches were adopted to ensure a consistent and meaningful assessment: (i) slabs with identical thickness (230 mm), and (ii) slabs with equivalent concrete volume (2.6 m^3), represented by the 160 mm thick solid slab and all voided slab configurations. The key findings of the study are summarized as follows:

- Thermal response: All slab configurations exhibit similar global temperature distributions, characterized by a steep gradient from the exposed surface toward the top. Void geometry has a limited influence on the overall temperature profile but introduces localized variations around the void regions.
- Effect of fire exposure: Midspan deflection increases systematically with increasing fire duration for all slab types, reflecting progressive degradation of material stiffness at elevated temperatures.
- Comparison based on identical thickness (230 mm): The 230 mm thick solid slab (3.7 m^3) exhibits the lowest deflection values due to its higher flexural stiffness. Voided

slabs of the same thickness show higher deflections as a result of reduced effective stiffness caused by internal voids.

- Comparison based on equivalent concrete volume (2.6 m^3): Voided slabs demonstrate lower deflections than the 160 mm thick solid slab, indicating that similar or improved deformation performance can be achieved using the same amount of concrete.
- Influence of volume reduction and material efficiency: Compared to the 230 mm solid slab (3.7 m^3), voided slabs reduce the concrete volume to 2.6 m^3, corresponding to an approximate 30% reduction. This demonstrates the effectiveness of voided slab systems in achieving significant material savings. Despite this reduction, the increase in deflection of voided slabs relative to the 230 mm solid slab remains moderate at ambient and early fire exposure stages, ranging approximately from 11–20% at ambient conditions and 16–28% after 30 min. At higher fire durations, this difference becomes more pronounced, increasing to approximately 21–42% at 90 min due to accelerated stiffness degradation at high temperatures.
- Stiffness degradation behavior: The stiffness degradation of voided slabs under fire exposure exhibits a two-stage response. During the initial phase (up to 30 min), voided slabs show comparable or slightly lower rates of degradation relative to the 160 mm solid slab, indicating stable structural response at early stages. However, with prolonged fire exposure, a transition occurs, and voided slabs exhibit a more pronounced increase in deformation, reflecting accelerated stiffness loss. This behavior is attributed to the combined effect of temperature penetration and reduced effective stiffness due to internal voids. Consequently, while voided slabs perform efficiently at early stages, their sensitivity to stiffness degradation becomes more significant under extended high-temperature exposure.
- Effect of void geometry: Elliptical and ellipsoidal void configurations exhibit marginally lower deflections, suggesting a more uniform stress distribution, whereas capsule and biaxial capsule geometries show relatively higher deformation, likely due to less favorable concrete distribution and localized stress concentrations.

Overall, the results demonstrate that voided slab systems provide a structurally efficient solution by reducing concrete volume while maintaining satisfactory deformation performance. However, their behavior reflects a trade-off between material efficiency and structural stiffness, particularly under prolonged fire exposure. Therefore, both geometric stiffness and material optimization should be considered in the fire-resistant design of voided slab systems.

From a design perspective, the results highlight a trade-off between material efficiency and residual stiffness. Voided slabs can achieve comparable performance with reduced concrete volume, particularly after moderate fire exposure; however, their increased sensitivity to severe fire exposure should be considered in design. Accordingly, both absolute deformation and relative degradation should be evaluated in assessing post-fire structural performance.

The present study adopts a simplified post-fire assessment framework in which residual material degradation is defined based on fire exposure, while the structural response is evaluated after assumed cooling to ambient conditions. Explosive spalling and residual stresses from the heating–cooling cycle were not considered and should be addressed in future studies. Incorporating full thermal cycles and extending the analysis to probabilistic frameworks [35] would enable more comprehensive assessment of post-fire structural reliability.

Author Contributions: Conceptualization, N.K. and M.Ö.; methodology, N.K. and M.Ö.; software, N.K.; validation, N.K.; formal analysis, N.K.; investigation, N.K.; writing—original draft preparation, N.K.; writing—review and editing, M.Ö.; supervision, M.Ö. All authors have read and agreed to the published version of the manuscript.

Funding: This research received no external funding.

Institutional Review Board Statement: Not applicable.

Informed Consent Statement: Not applicable.

Data Availability Statement: The data presented in this study are available on request from the corresponding author.

Conflicts of Interest: The authors declare no conflicts of interest.

References

1. Churakov, A. Biaxial hollow slab with innovative types of voids. *Stroit. Unikal'nyh Zdanij Sooruz.* **2014**, *6*, 70.
2. Dwivedi, A.K.; Joshi, P.H.; Raj, R.; Mishra, P.P.; Kadhane, M.; Mohabey, B. Voided slab design Voided Slab Design: Review Paper. In Proceedings of the 3rd International Conference on Multidisciplinary Research & Practice, Ahmedabad, India, 24 December 2016; Volume 4, pp. 220–226.
3. Siti Quraisyah, A.D.; Kartini, K.; Hamidah, M.S.; Daiana, K. Bubble deck slab as an innovative biaxial hollow slab—A review. *J. Phys. Conf. Ser.* **2020**, *1711*, 012003. [CrossRef]
4. Suman, S.; Mukherjee, S.; Roy, D.K.S. A comparative review on bubble-voided reinforced concrete slab—An innovative concept for lightweight concreting. *Mater. Today Proc.* 2023, *in press*. [CrossRef]
5. Gamal, M.; Heiza, K.; Hekal, G.; Nabil, A. Voided slabs as a new construction technology—A review. *Int. J. Adv. Struct. Geotech. Eng.* **2025**, *9*, 94–118. [CrossRef]
6. Omar, A.A.A.A.A. A state of the art review on reinforced concrete voided slabs. *ARPN J. Eng. Appl. Sci.* **2018**, *13*, 1678–1700.
7. Hussein, L.F.; Al-Taai, A.A.S.; Khudhur, I.D. Sustainability achieved by using voided slab system. *AIP Conf. Proc.* **2020**, *2213*, 020071. [CrossRef]
8. Staszak, N.; Garbowski, T.; Ksit, B. Optimal design of bubble deck concrete slabs: Sensitivity analysis and numerical homogenization. *Materials* **2023**, *16*, 2320. [CrossRef]
9. Schnellenbach-Held, M.; Pfeffer, K. Punching behavior of biaxial hollow slabs. *Cem. Concr. Compos.* **2002**, *24*, 551–556. [CrossRef]
10. Lai, T. Structural Behavior of BubbleDeck® Slabs and Their Application to Lightweight Bridge Decks. Ph.D. Thesis, Massachusetts Institute of Technology, Cambridge, MA, USA, 2010.
11. Subramanian, K.; Bhuvaneshwari, P.; Jabez, N.A. Flexural behaviour of biaxial slabs voided with spherical HDPP void formers. *Iran. J. Sci. Technol. Trans. Civ. Eng.* **2017**, *41*, 373–381. [CrossRef]
12. Valivonis, J.; Šneideris, A.; Šalna, R.; Popov, V.; Daugevicius, M.; Jonaitis, B. Punching strength of biaxial voided slabs. *ACI Struct. J.* **2017**, *114*, 1373–1383. [CrossRef]
13. Sagadevan, R.; Rao, B.N. Experimental and analytical investigation of punching shear capacity of biaxial voided slabs. *Structures* **2019**, *20*, 340–352. [CrossRef]
14. Sagadevan, R.; Rao, B.N. Flexural behavior of reinforced concrete biaxial voided square slabs. *ACI Struct. J.* **2020**, *117*, 3–14. [CrossRef]
15. Pawar, A.J.; Mathew, N.S.; Dhake, P.D.; Patil, Y.D. Flexural behavior of two-way voided slab. *Mater. Today Proc.* **2022**, *65*, 1534–1545. [CrossRef]
16. Huang, Z. The behaviour of reinforced concrete slabs in fire. *Fire Saf. J.* **2010**, *45*, 271–282. [CrossRef]
17. Schneider, U. Concrete at high temperatures—A general review. *Fire Saf. J.* **1988**, *13*, 55–68. [CrossRef]
18. Hertz, K.D. Concrete strength for fire safety design. *Mag. Concr. Res.* **2005**, *57*, 445–453. [CrossRef]
19. Ma, Q.; Guo, R.; Zhao, Z.; Lin, Z.; He, K. Mechanical properties of concrete at high temperature—A review. *Constr. Build. Mater.* **2015**, *93*, 371–383. [CrossRef]
20. Al-Gasham, T.S.; Alawsi, M.A.; Mhalhal, J.M.; Abid, S.R. Damage assessment of RC voided slabs experienced extreme fire flame. *IOP Conf. Ser. Mater. Sci. Eng.* **2021**, *1058*, 012051.
21. Strahm, B.; Haufe, C.N.; Blandini, L. Investigations of the fire behavior of functionally graded concrete slabs with mineral hollow spheres. *Fire* **2024**, *7*, 256. [CrossRef]
22. Al-Gasham, T.S.; Mhalhal, J.M.; Al-Magsusy, L.J. Bubble slabs burned at 800 °C with different periods. *IOP Conf. Ser. Mater. Sci. Eng.* **2021**, *1058*, 012058. [CrossRef]

23. Miller, O.; Gericke, O.; Nigl, D.; Kovaleva, D.; Blandini, L. Simulation-based investigations of the load-bearing behavior of concrete hollow sphere slabs exposed to fire. *Fire* **2022**, *5*, 197. [CrossRef]
24. *ISO 834-1:1999*; Fire Resistance Tests—Elements of Building Construction—Part 1: General Requirements. International Organization for Standardization: Geneva, Switzerland, 1999.
25. ANSYS, Inc. *ANSYS Workbench*, version 2022 R1; ANSYS Inc.: Canonsburg, PA, USA, 2022.
26. *EN 1992-1-2:2004*; Eurocode 2: Design of Concrete Structures—Part 1-2: Structural Fire Design. European Committee for Standardization (CEN): Brussels, Belgium, 2004.
27. *EN 1993-1-2:2005*; Eurocode 3: Design of Steel Structures—Part 1-2: Structural Fire Design. European Committee for Standardization (CEN): Brussels, Belgium, 2005.
28. *EN 1991-1-2:2002*; Eurocode 1: Actions on Structures—Part 1-2: Actions on Structures Exposed to Fire. European Committee for Standardization (CEN): Brussels, Belgium, 2002.
29. BubbleDeck International. BubbleDeck Technical Manual. Available online: https://www.bubbledeck-uk.com/pdf/2-BDTechManualv1a.pdf (accessed on 7 May 2026).
30. *EN 1991-1-1:2002*; Eurocode 1: Actions on Structures—Part 1-1: General Actions. European Committee for Standardization (CEN): Brussels, Belgium, 2002.
31. Khan, A.A.; Usmani, A.; Torero, J.L. Evolution of fire models for estimating structural fire-resistance. *Fire Saf. J.* **2021**, *124*, 103367. [CrossRef]
32. Beneš, M.; Štefan, R. Hygro-thermo-mechanical analysis of spalling in concrete walls at high temperatures as a moving boundary problem. *Int. J. Heat Mass Transf.* **2015**, *85*, 110–134. [CrossRef]
33. Jansson, R. Material Properties Related to Fire Spalling of Concrete. Licentiate Thesis, Division of Building Materials, LTH, Lund University, Lund, Sweden, 2008.
34. Ranjbar, F.; Asgari, A.; Bagheri, M.; Bengar, H.A. Insights into the mechanisms and seismic performance of reinforced concrete buildings on a pile foundation in liquefiable deposits. *Structures* **2026**, *87*, 111557. [CrossRef]
35. Akbarzadeh, M.R.; Pourhanasa, R.; Bahmanpour, A.; Ranjbar, F.; Asgari, A. Multi-dimensional seismic fragility assessment of steel diagrid systems under mainshock–aftershock sequences via vine-copula modeling. *Soil Dyn. Earthq. Eng.* **2026**, *206*, 110267. [CrossRef]

Disclaimer/Publisher's Note: The statements, opinions and data contained in all publications are solely those of the individual author(s) and contributor(s) and not of MDPI and/or the editor(s). MDPI and/or the editor(s) disclaim responsibility for any injury to people or property resulting from any ideas, methods, instructions or products referred to in the content.